RSC Mechanochemistry

ROYAL SOCIETY OF CHEMISTRY

PAPER

View Article Online
View Journal | View Issue

Cite this: *RSC Mechanochem.*, 2026, **3**, 67

Mechanochemical reduction of nickel oxide with continuous hydrogen flow

Jikai Ye, [a] Gang Liu,[b] Christian H. Liebscher [bc] and Michael Felderhoff *[a]

Metal oxides reduction is one of the most important steps in metal production, where hydrogen-based metallurgy would significantly reduce greenhouse gas emissions from this emission-intensive process. By using mechanical energy, mechanochemistry enables the reduction of metal oxides at lower temperatures or even room temperature, which could significantly reduce energy loss due to heat dissipation in metal production at high temperatures. However, increased water partial pressure from hydrogen-based reduction leads to limited reaction rates. Herein, we demonstrate a mechanochemical method for the reduction of nickel oxide, adopting a ball milling system under continuous hydrogen flow. Nickel oxide can be mechanochemically reduced at room temperature or with mild heating (100 °C) for faster water removal. 88 wt% of nickel could be reduced after 10 h of milling. Efficient mechanochemical reduction benefits from the generation of abundant oxygen vacancies, increased surface area, continuously renewed particle surface, and constant removal of moisture. Compared to traditional metal oxide reduction methods, hydrogen-based mechanochemical reduction offers a low-temperature metallurgical pathway with no direct carbon emissions.

Received 30th June 2025
Accepted 25th September 2025

DOI: 10.1039/d5mr00089k

rsc.li/RSCMechanochem

Introduction

Humankind has benefited from metallurgy since ancient times, by extracting metals from naturally occurring minerals for use in production, manufacturing, construction, and other applications. Traditional metallurgical processes require high temperature for faster mass transfer and favorable thermodynamics. However, these processes are highly energy-intensive, which contributes to metal production accounting for 10% of the world's total energy consumption.[1,2] In addition, the use of carbonaceous materials as reducing agents leads to substantial CO_2 emissions, contributing nearly 40% of the world's total industrial greenhouse gas emissions.[2,3]

To reduce CO_2 emissions during metallurgical processes, technologies such as direct reduction with hydrogen gas[4–6] and hydrogen-based plasma in electrical arc furnaces[7–9] have received more attention in recent years. With hydrogen as reducing agent, the reduction process is emission-free as the only byproduct is water. When the hydrogen is produced through electrolysis powered by renewable energy, the entire process becomes "green". However, due to the thermodynamic stability of metal oxides and sluggish reaction kinetics, an overall high temperature is still needed for efficient metal oxides reduction.[5,7]

Mechanochemistry, as was identified by IUPAC as one of the most promising technologies for a sustainable future,[10] might provide energy-efficient solutions. The term describes chemical reactions, typically solid–state reactions, enabled by mechanical energy input, such as manual grinding, ball milling, twin-screw extrusion, resonant acoustic mixing, spray drying, *etc.* These reactions can take place under much milder conditions (lower temperature, lower pressure, less solvent), benefiting from the distorted symmetry within molecules, breaking of bonds, formation of defects, *etc.* under mechanical impacts.[11–14] Mechanochemistry has a long history as a metal production method. Since antiquity, humans have employed this method to extract mercury with copper from ores.[15,16] Modern applications have been extended to mechanical alloying.[17–19] Metal oxide reduction can also be realized *via* mechanochemistry. Either carbon[20,21] or metals/metal composites with higher reactivities[22–26] can be used as reductants. While carbonaceous reductants still bring emissions of greenhouse gases, reactive metals/metal composites are often difficult to be produced in the first place. Yet, the ultimate goal remains to be hydrogen-based reduction of metal oxides.

In this study, mechanochemical reduction of metal oxides with hydrogen is investigated with NiO as a model oxide. Nickel plays an important role in human life and exists in nature mostly in the form of oxides as laterites. In addition, the reduction of nickel oxide is an important step in nickel production, as nickel oxide is often a key intermediate in the

[a]*Max-Planck-Institut für Kohlenforschung, Department of Heterogeneous Catalysis, 45470 Mülheim an der Ruhr, Germany. E-mail: felderhoff@mpi-muelheim.mpg.de*
[b]*Max Planck Institute for Sustainable Materials, 40237 Düsseldorf, Germany*
[c]*Research Center Future Energy Materials and Systems & Faculty of Physics and Astronomy, Ruhr University Bochum, 44801 Bochum, Germany*

metallurgical routes of nickel, regardless from laterite or sulfide ores.[27] Furthermore, the reaction of nickel oxide with hydrogen itself is a single-stage reduction due to the simplicity of Ni–O phase diagram,[28,29] which makes it easier to study and a good model reaction to pave ways for general metal oxides reduction.

The thermal reduction of nickel oxide with hydrogen has been studied to a good extent, despite that due to varieties of experimental conditions, diverse observations were made such as different applicable kinetic models or observable induction period.[30,31] The reduction of NiO is shown as reaction (1), and is typically performed at temperatures as high as 250–1300 °C, due to its sluggish kinetics at low temperatures.[31,32]

$$NiO + H_2 \rightarrow Ni + H_2O \quad (1)$$

The initial reduction of NiO with hydrogen generally occurs at the surface *via* the generation of oxygen vacancies.[33–36] This stage sometimes appears as an induction stage especially under low pressure and/or at low temperature. As the concentration of oxygen vacancies increases, reduced nickel particles grow and H_2 is more easily adsorbed and dissociated,[36] and the reduction rate therefore significantly increases. The reduction process then becomes diffusion-controlled, requiring hydrogen to diffuse into the bulk material, while oxygen must exit either through oxygen vacancies or in the form of water molecules.[32,37] The generated water slows the process by absorbing on the surface of nickel particles, prohibiting H_2 dissociation, as well as blocking the diffusion pathways.[33,37]

In earlier attempts for mechanochemical reduction of NiO, carbon[38] or reactive metals such as Mg,[39] Ti,[39,40] Al,[41,42] Li [43] were investigated to reduce NiO mechanochemically, benefited from the thermodynamic stability of their respective oxides. However, due to the same reason, the production of these reactive metals is generally emission- and/or energy-intensive. Doppiu *et al.*[44] have achieved controlled reduction of NiO *via* ball milling at room temperature for the first time with H_2. However, only a maximum of ~29 wt% of Ni was reduced from NiO with H_2 after pre-milling NiO under Argon atmosphere for a total of 20 h. The generated water vapor was believed to be the key factor that limits the reduction rate by reducing the diffusion of hydrogen into Ni layer and the outward diffusion of water molecules, similar to the cases in thermal reduction.

Herein, to promote sustainable reduction of NiO with low temperature and low CO_2 emissions, we report an efficient mechanochemical method to reduce NiO with hydrogen. With the help of continuous H_2 flow at ambient pressure, water generated from reduction reaction can be removed. Benefited from increased surface area, shortened diffusion distances, consistently renewed particle surfaces, and continuous removal of generated water, NiO could be much more efficiently reduced.

Results and discussion

Room-temperature reduction of nickel oxide with reactive ball milling

To confirm the feasibility of mechanochemical reduction of NiO, NiO was first ball milled in a planetary mill using a tungsten carbide (WC) jar and balls under hydrogen pressure. The powder X-ray diffraction (XRD) pattern (Fig. 1) confirms that the initial NiO particles show characteristic peaks at 2θ = 16.9°, 19.6°, 27.8°, 32.7°, 34.2°, 39.7°, 43.4°, 44.6°, and 49.2°, corresponding to {111}, {200}, {220}, {311}, {222}, {400}, {331}, {420}, and {422} planes of face-centered cubic (fcc) NiO (ICDD No. 00-004-0835), respectively. After 10 h of milling under 50 bar H_2 at room temperature, peaks corresponding to {111}, {200}, {220}, {311}, {222}, and {400} planes of fcc Ni (ICDD No. 00-004-0850) at 2θ = 20.1°, 23.2°, 33.1°, 39.0°, 40.8°, and 47.5° appear, which indicates the reduction of NiO at room temperature. Mechanical impacts typically create abundant defects by breaking chemical bonds and promoting the mobility of atoms.[11,12,45,46] In the case of metal oxides, oxygen vacancies can be created mechanochemically, especially with the existence of reductants.[44,47–50] Oxygen vacancies have been proven crucial for the reduction process, especially in the early stage known as the induction perfiod.[36,51] The observable peak broadening of the XRD patterns from the milled samples, compared to the starting material NiO, suggests a decrease in crystallite size, due to the fragmentation of particles and introduction of defects caused by mechanical energy. The downsizing of particles helps reveal more surface that is available for further mechanical impacts. However, even with increasing milling time of 20 h, the Bragg peaks of NiO remain much more prominent than those for Ni, with the peaks at 2θ = 16.9°, 19.6°, and 27.8°, which corresponds to the {111}, {200}, and {220} planes of NiO, respectively, still being the strongest peaks. A further increase of milling time to 50 h and hydrogen pressure to 100 bar still resulted in poorly reduced Ni. Rietveld refinement of the XRD results suggest that the amount of Ni were only 7 wt%, 15 wt%, and 19 wt% after 10 h, 20 h, and 50 h of milling, respectively. This suggests a low reaction rate for the overall reduction. The reason for the limited reaction yield is assumed to be the increase in the water partial pressure in the closed milling jar, as was also observed by Doppiu *et al.*[44] Absorbed water molecules hinder the diffusion of hydrogen and oxygen species.[44,52]

To partly remove the generated water from the closed system and further confirm the influence of water partial pressure on

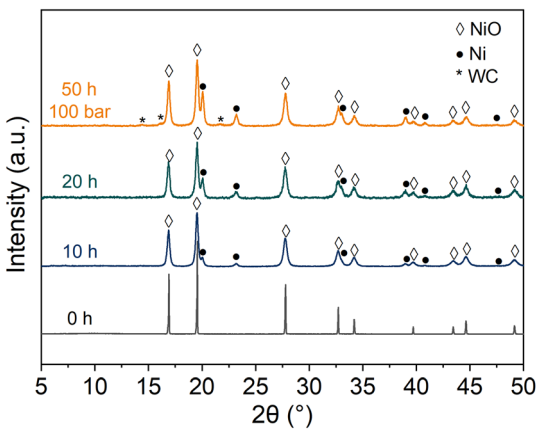

Fig. 1 XRD patterns of NiO powders milled for 0, 10, 20 h under 50 bar H_2 and 50 h under 100 bar H_2 in a planetary mill at room temperature.

NiO reduction, several evacuation sessions were performed during the milling process to renew the reaction atmosphere. After every 10 h of milling, the milling jar was evacuated under dynamic vacuum for 1 h *via* a Schlenk line and then refilled with dry hydrogen to remove moisture from the closed system. This process was repeated four times, resulting in a total milling time of 50 h. As confirmed by XRD results (Fig. 2), peaks corresponding to Ni became much stronger, with the peak at $2\theta = 20.1°$ (Ni {111}) becoming the strongest, signaling that significantly more NiO was reduced after moisture removal by the evacuation sessions. Rietveld refinement of the XRD pattern confirms that 56 wt% of Ni was reduced, which proves the decisive effect of water in terms of reduction rate.

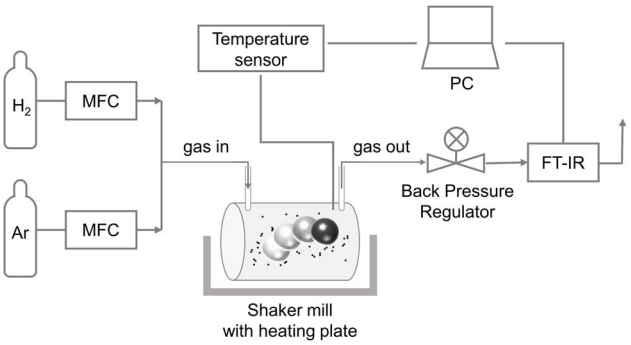

Fig. 3 Schematic illustration of the continuous gas-flow ball milling system.

Improved reduction of nickel oxide with continuous hydrogen flow

Given the crucial role of water partial pressure in metal oxide reduction, a continuous gas-flow ball milling system[53] was then used for NiO reduction, with the aim of uninterrupted removal of water with H_2 flow. This was achieved by a modified Retsch MM400 shaker mill, in which home-built stainless-steel jars are equipped with gas connections. As illustrated in Fig. 3, the system is also equipped with a heating plate, a back-pressure regulator, and a Fourier-Transform Infrared (FT-IR) Spectrometer, which enables heating, back-pressure regulation, and real-time analysis of the gas phase product, respectively. For further details of this set-up, readers are referred to our previous work.[53]

Due to the increased surface area of ball-milled materials and the significant water affinity of NiO,[54] the H_2O produced from the reduction process can be easily absorbed on the surface of the powders. To accelerate water desorption during milling, a mild heating (100 °C) was applied. The temperature was recorded at the interior upper wall of the jar and the temperature profile is shown in Fig. S1. Real-time FT-IR spectra (Fig. 4) of the exhaust gas show a noticeable removal of moisture with the appearance of absorption peaks between 4000–3000 cm^{-1} and 2300–1300 cm^{-1}, which are characteristic peaks corresponding to water.[55] After 1 h of milling, the spiky peaks representing moisture began to appear by pointing upwards, indicating a decreased amount of moisture in the exhaust gas compared to the reference measured before milling began. Despite a very pure H_2 gas source (99.999%), additional moisture can be introduced along the pipelines. The reason for a less moist exhaust gas after 1 h could be the result of particle size reduction of the highly hydrophilic NiO,[54] which leads to a larger surface area and thus more surface adsorption sites. It could also be a result of the reaction between moisture and steel, consuming water and generating hydrogen *via* ball milling.[56] After 2 h of milling, a small amount of CO_2 (~2356 cm^{-1}) was detected, which should be desorbed from the NiO particles and stainless steel after milling began. The absorbed CO_2, together with other carbon species in the steel and/or PTFE gasket ring, also leads to a small amount of CH_4 (~3020 cm^{-1}) after hydrogenation,[53] where steel and/or Ni–NiO can serve as catalysts.[57,58] As milling progresses, more water is generated and carried away by the H_2 gas flow. After about 5 to 6 h, the moisture content of the exhaust gas reached a peak. Although the reaction rate did not necessarily peak until then, the subsequent decrease in moisture content indicates an advancement of the reaction.

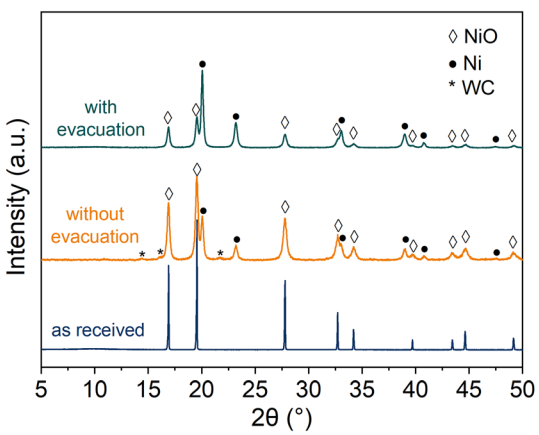

Fig. 2 XRD patterns of NiO powders milled under 100 bar H_2 for 50 h in a planetary mill, with and without evacuation sessions in between. Initial NiO is provided as reference.

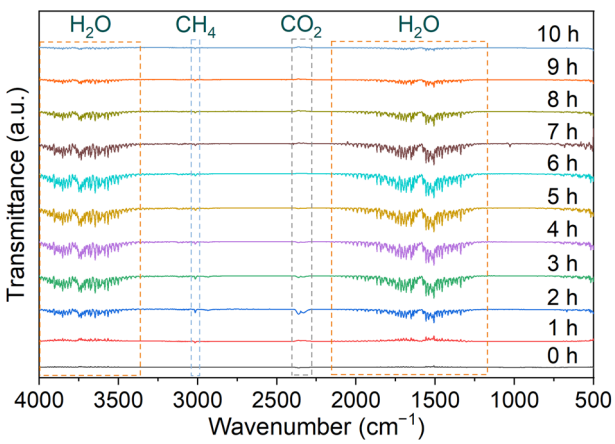

Fig. 4 Real-time FT-IR Spectra of the exhaust from milling NiO with a H_2 flow of 30 mL min^{-1} at 100 °C.

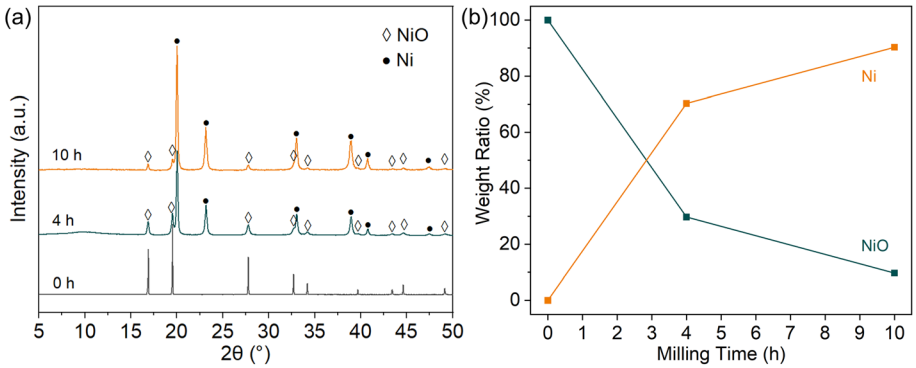

Fig. 5 (a) XRD patterns of NiO–Ni powders for different milling times under H_2 flow and (b) NiO/Ni content development at different milling times.

The extent of reduction is indicated by powder XRD patterns after different reaction times, as shown in Fig. 5a. The peaks at $2\theta = 20.1°$, and 23.2°, corresponding to {111}, and {200} planes of Ni, became the strongest peaks only after 4 h of milling, which is in stark contrast to the case with the closed system (see Fig. 1). After 10 h of milling, most of the diffraction peaks corresponding to NiO became significantly weaker with some being barely identifiable, which signifies a decrease in the amount of NiO. The ratio between NiO and Ni, as shown in Fig. 5b, was derived from Rietveld refinement of the XRD results. After 4 h, approximately 65 wt% of Ni was reduced, and after 10 hours, 88 wt%. This indicates a much faster reaction rate and an improved reduction extent compared to the closed system.

The particle size and morphology development of Ni–NiO species were investigated using Scanning Electron Microscopy (SEM) and Transmission Electron Microscopy (TEM). As shown in Fig. S2, the commercial NiO particles (325 mesh, 99%, Alfa Aesar) are generally in the size of several micrometer to several tens of micrometer, exhibit a relatively smooth surface, and tend to agglomerate. This morphology is typical when thermal treatment is part of the synthesis process.[59,60] During the milling process, the particle size reduced significantly to the nanometer range, and the surface also became more uneven due to mechanical interactions, as shown in Fig. S3–S5 shows typical overviews of particles under TEM. After 4 h of milling, Ni–NiO particles have a mean particle diameter (geometric mean) of 105 nm, and it became 76 nm when the milling time was extended to 10 h. It is worth noting, however, that observations under TEM may have the tendency towards smaller and less magnetic particles in the sample, which may lead to bias in determining particle size. A reduced particle size leads to an increased surface area. As suggested by N_2 physisorption (Fig. S6), commercial NiO has a BET surface area of <4 $m^2\ g^{-1}$, which is a typical value for non-porous materials in the micrometer range. After 4 h of milling, it increased to about 17 $m^2\ g^{-1}$. While after 10 h of milling, the BET surface area decreased slightly to 13 $m^2\ g^{-1}$. The pattern of the surface area change, characterized by an initial increase followed by a decrease, is not uncommon in mechanical treatment.[61,62] In this case, the increase in surface area is mainly driven by the fragmentation of large NiO particles, which is beneficial for mechanochemical reactions, as mechanical forces are mainly applied directly at the surface of particles. A later decrease in surface area is possibly derived from particle growth of Ni due to cold welding.

Control experiments were performed to confirm that the reduction of NiO at 100 °C was mechanically-driven instead of thermally-driven. Same as in the closed planetary milling system, room-temperature reduction was possible under H_2 flow in the shaker mill. As shown in Fig. S7(a), the peak at $2\theta = 20.1°$, corresponding to {111} planes of Ni in the XRD pattern, was the strongest after 11 h of milling, suggesting a higher reduction level with hydrogen flow than in the closed milling system. Rietveld refinement of the XRD pattern confirms that 62 wt% Ni was reduced at room temperature with H_2 flow, which is much higher than that from a closed system. Due to slower moisture removal, the reduction rate is slower than that at 100 °C. Fig. S7(b) shows the real-time FT-IR spectra of the exhaust gas from the NiO reduction with H_2 flow at room temperature. The signals of water show similar but delayed pattern as those observed with mild heating, as a result of slower water desorption and therefore slower reaction rate. After 3 h of milling, the water level in the exhaust increased, compared to the reference value recorded at the beginning of the reaction. After 11 h of milling, the peaks corresponding to water were still prominent, which shows delayed reaction progress relative to the case with heating. The increase of the jar temperature due to friction was monitored, as shown in Fig. S8. The temperature of the jar increased to about 32 °C after 2 h of milling and stayed dynamically stable afterwards. These results suggest that at room temperature (without heating), NiO reduction with hydrogen flow develops the same way as with heating, only at a lower rate because of slower water desorption. By shaking in the milling jar without balls with the same frequency at 100 °C under H_2 flow, no reduction of NiO was observed by XRD after 14 h of shaking, as shown in Fig. S9. By first milling under Ar, then heating under H_2, the sole effect of size reduction from ball milling was tested out. Only a small amount of NiO was reduced to Ni and/or iron-nickel alloy, as shown in Fig. S10, likely due to the reaction with iron from stainless steel. The possibility of nickel oxide reduction with

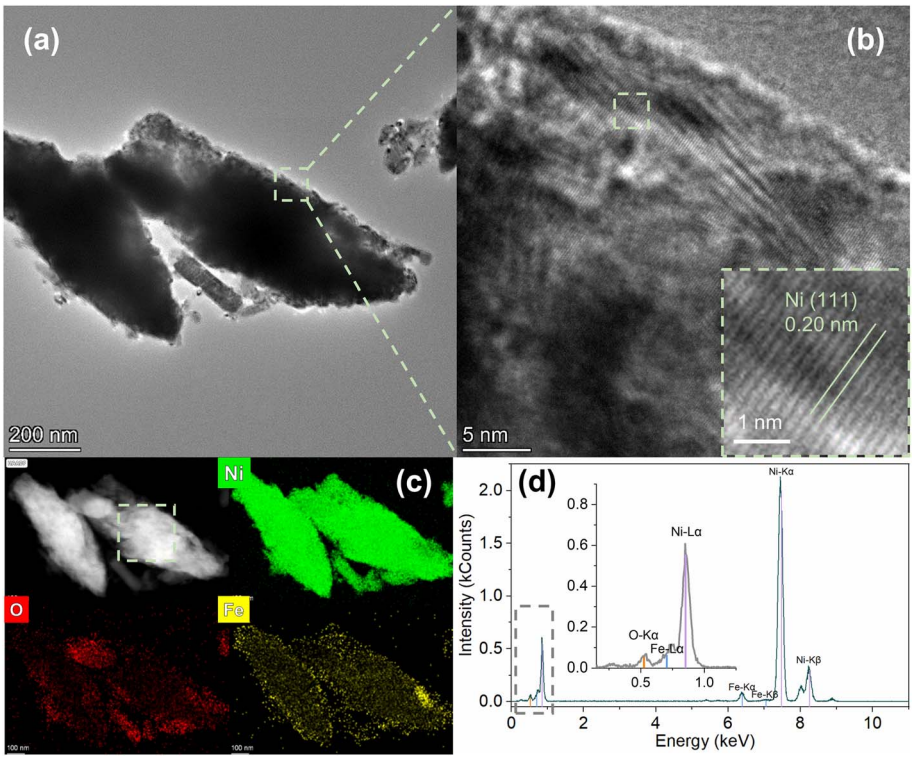

Fig. 6 (a) TEM image of typical Ni particles after 10 h of milling. (b) High-resolution TEM image of the selected area in (a), with an enlarged view of the selected area in (b) as inset. (c) STEM-EDX elemental mapping of the particles. The gray scale image represents the corresponding HAADF-STEM image. (d) EDX spectrum of the selected area in (c), with an enlarged view of the O–K_α and Ni–L_α X-ray energy range in (d) as inset.

iron is further confirmed by Fig. S11. These results suggest that, even with the size reduction effect from ball milling, temperature as low as 100 °C is not sufficient for thermally-driven reduction of NiO.

In order to get more information about the reduction process, the distribution of Ni-species was investigated by Energy Dispersive X-ray (EDX) Spectroscopy equipped in a TEM. Doppiu *et al.*[44] have observed a core–shell structure while mechanochemically reducing NiO, suggesting a surface reduction process. Although no obvious radial distribution of nickel or oxygen content was observed in our measurement, as shown in Fig. S12, it is believed that reduction first takes place at the surface of the NiO particles due to collisions among the surface of particles, balls, and the jar. Iron elements come from abrasion of stainless steel milling jar and balls. Compared to that of 4 h, at 10 h of reaction time, separated metal oxide and metal particles could be observed. TEM images and EDX mapping with higher resolution reveal clear distinction between oxide particles (Fig. S13) and reduced particles (Fig. 6), suggesting a separation of Ni after being reduced from NiO. In a thermal reduction scenario, reduced Ni often forms at the surface of NiO, thus hindering the mass transfer of hydrogen and oxygen-species.[31,34] The separation of Ni from NiO during mechanochemical reduction is likely the result of cold welding from metal–metal contact among the reduced Ni at the surface of NiO particles.[63] As ball-milling process promotes particle movement and interaction, metallic Ni is more easily welded onto each other and grows into individual particles. This is beneficial for further reduction as it continuously renews the surface and reveals more NiO.

Based on the aforementioned observations, the proposed NiO–Ni particle evolution during mechanochemical reduction is schematically illustrated in Fig. S14. In the first stages of ball milling, the initial NiO powder particles are first fragmented to smaller particles, which provides larger surface area and therefore more available sites for both mechanical impacts and hydrogen adsorption. The formation of defects especially oxygen vacancies induced by mechanical forces promotes the reduction reaction. The O atoms are taken by H_2, turning into H_2O. The thus-revealed nickel sites surround oxygen vacancies further help H_2 dissociation into H atoms and diffuse at the surface. The surface of the particles could be first reduced to Ni with mechanical energy input. As the particles constantly collide, the reduced Ni is cold-welded with each other and subsequently detaches from NiO, leading to the formation and growth of Ni particles. This helps reveal fresh surface of NiO and hence promote further reduction of NiO. Benefiting from the H_2 flow, the partial pressure of H_2O remains low. Compared to the closed system, the generated H_2O can desorb more easily from the surface of the particles. The absorbed water layer is minimized especially with mild heating, minimizing the hindrance to the diffusion of hydrogen and oxygen species.

Fig. 7 illustrates the comparison between thermal reduction and mechanochemical reduction of NiO. During a typical

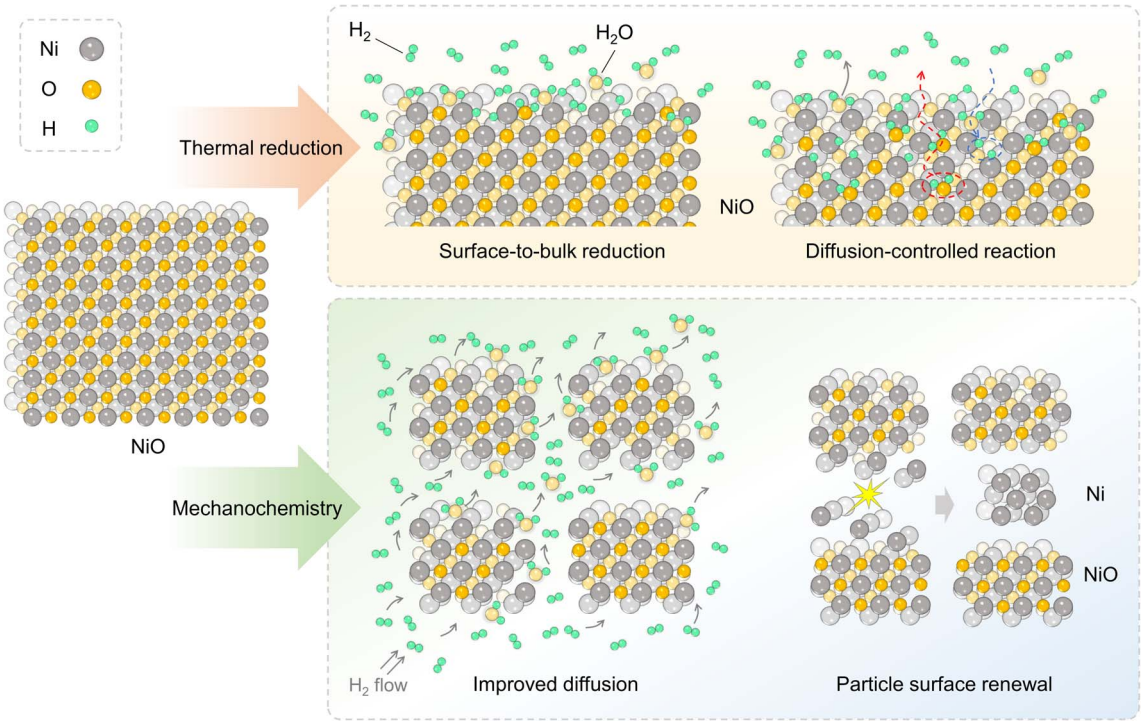

Fig. 7 Schematic illustration of mechanochemical reduction of NiO in comparison to thermal reduction.

thermal reduction, the reduction of NiO follows a Ni nucleation – pore formation – Ni densification scheme, the reduction of NiO follows a surface-to-bulk pattern and NiO is often trapped inside Ni, suffering from a deteriorated diffusion.[31,34] In the mechanochemical scenario, the penetration depth required for hydrogen is greatly reduced due to downsize effect from ball-milling, which contributes to improved kinetics. Consequently, cold welding and particle growth of Ni renews the surface of particles and reveals more unreduced NiO, continuously improving the mass transfer. Additionally, benefiting from the continuous atmosphere renewal from H_2 flow enabled by the gas-flow milling system, water partial pressure in the milling jar is controlled, enabling a better reaction rate as compared to a closed system.

Experimental

Room-temperature reduction of nickel oxide with reactive ball milling

800 mg NiO (325 mesh, 99%, Alfa Aesar) as well as tungsten carbide milling balls with a ball-to-powder ratio of 40 : 1 were put in a tungsten carbide milling jar with a volume of 30 mL. The atmosphere inside the jar was first replaced with Argon *via* Schlenk line for 3 times. Additional 50 or 100 bar H_2 (99.999 mol%, Air Liquide, Alphagaz 1) was then charged into the jar. A planetary ball mill (Pulverisette 6, Fritsch) was used for 0, 10, 20, or 50 h at a rotation speed of 450 rpm, with 10 min pause for every 30 min of milling to mitigate temperature increase of the system. The evacuation process was conducted by releasing the pressure after every 10 h of milling and evacuating dynamically for 1 h before filling ambient-pressure Ar and recharging hydrogen.

Reduction of nickel oxide with continuous hydrogen flow

800 mg NiO (325 mesh, 99%, Alfa Aesar) as well as stainless steel milling balls with a ball-to-powder ratio of 30 : 1 were put in a stainless steel milling jar with a volume of 23 mL. The atmosphere was first replaced by purging with 30 mL min^{-1} H_2 (99.999 mol%, Air Liquide, Alphagaz 1) for 1 h. A shaker mill (MM400 mixer mill, Retsch) was then used for continuous milling with a shaking frequency of 18 Hz, where it was heated up to 100 °C with a heating plate below the jar. H_2 flow was kept constant at 30 mL min^{-1}. Another experiment was done without heating.

To rule out thermally-driven reduction, NiO was shaken at 18 Hz without balls for 14 h at 100 °C under 30 mL min^{-1} H_2 flow. Additionally, NiO was also first milled under 20 mL min^{-1} Ar at room temperature for 8 h, and subsequently heated without milling under 30 mL min^{-1} H_2 at 100 °C for 8 h.

Material characterizations

The phase composition of powdery samples was characterized by powder X-ray diffraction (XRD, STOE STADI P transmission diffractometer) with Mo Kα (λ = 0.7093 Å). The instrument is equipped with a primary Ge(111) monochromator (Mo Kα1) and a position-sensitive Mythen1K detector. Data were acquired in the range between 2θ of 5 and 50° with a step size of 0.015°. The measurement time was 20 seconds per step. Samples were filled into glass capillaries (D0.5 mm) for measurements.

Fourier-Transform Infrared (FT-IR) spectra of the product gas stream were collected in transmission mode on a Thermo Nicolet Avatar 370 FT-IR spectrometer equipped with a DTGS-detector and a 2 m flow cell (200 mL) heated to 150 °C. For each data point, 32 scans were measured with a resolution of 4 cm^{-1} in the 4000–500 cm^{-1} range.

Nitrogen physisorption was performed on a Micromeritics 3Flex at −196 °C. Prior to all measurements, the samples were degassed at 150 °C under vacuum (<1.33×10^{-2} mbar) for 12 h. Brunauer–Emmett–Teller (BET) surface area was calculated with the Micromeritics MicroActive software (version 5.02) in the relative pressure range of 0.05 to 0.30.

Particle morphology and lattice structures were characterized using scanning electron microscopy (SEM) and transmission electron microscopy (TEM). SEM was performed using Hitachi S-5500 at an acceleration voltage of 30 kV. TEM was performed employing both a JEOL 2100 F operating at 200 kV and an image-corrected Titan Themis G2 microscope at 300 kV, each equipped with energy-dispersive X-ray spectroscopy (EDS). Samples were prepared by dispersing dry powder onto a 400-mesh carbon lacey copper grid.

Conclusions

In conclusion, efficient mechanochemical reduction of nickel oxide has been realized by ball milling in hydrogen. Induced by constant mechanical impacts, nickel oxide can be reduced with hydrogen at room temperature. However, water generated during reduction accumulates in the system, gains partial pressure, absorbs on the surface of the particles, and thus hinders the diffusion of hydrogen, leading to a decreased reaction rate, with only 19 wt% Ni reduced after 50 h of milling under 100 bar H_2. With the continuous hydrogen flow, moisture is continuously taken away, which helps maintain a much higher reduction rate. With 30 mL min^{-1} H_2 flow at ambient pressure, 62 wt% Ni could be reduced after 11 h of ball milling at room temperature, and 88 wt% after 10 h of ball milling only with mild heating (100 °C). Compared to hydrogen-based thermal reduction, mechanochemical reduction benefits from abundant oxygen vacancies, increased surface area, consistently renewed particle surface, and therefore shortened mass transfer distance. Much lower temperature is required while good reduction rate is achieved. Compared to traditional metal oxide reduction methods, hydrogen-based mechanochemical reduction provides a low-temperature metallurgical pathway with no direct carbon emissions.

Author contributions

Jikai Ye: conceptualization, data curation, formal analysis, investigation, methodology, visualization, writing – original draft, writing – review & editing. Gang Liu: data curation, formal analysis, investigation, methodology, writing – review & editing. Christian H. Liebscher: supervision, methodology, writing – review & editing. Michael Felderhoff: conceptualization, methodology, supervision, writing – review & editing.

Conflicts of interest

There are no conflicts of interest to declare.

Data availability

All data presented in this paper are included in the main manuscript and the supplementary information (SI). Supplementary information is available. See DOI: **https://doi.org/10.1039/d5mr00089k**.

Acknowledgements

The authors acknowledge Dr Steffen Reichle for his help with the gas-flow ball milling system, Jan Ternieden, Dr Muzi Chen, and Prof. Dr Claudia Weidenthaler for XRD measurement and analysis, and fine mechanics workshop and pressure lab of MPI für Kohlenforschung for reactor manufacturing and high-pressure set-ups. We would also like to thank Volker Kree and Dr Eko Budiyanto for TEM measurement, Alexander Kostis and Aamir Abbas for SEM measurement, and Hannaneh Hosseini for TEM and N_2 physisorption measurement. Dr Christoph Somsen is acknowledged for fruitful discussions. Kateryna Peinecke and Dr Felipe Marques are acknowledged for critical reading of the manuscript. Jikai Ye acknowledges funding from International Max Planck Research School for Sustainable Metallurgy (IMPRS SusMet).

References

1 S. Seetharaman, *Fundamentals of Metallurgy*, Taylor & Francis, 2005.
2 D. Raabe, The Materials Science behind Sustainable Metals and Alloys, *Chem. Rev.*, 2023, **123**(5), 2436–2608.
3 J. M. Allwood, J. M. Cullen, M. A. Carruth, D. R. Cooper, M. McBrien, R. L. Milford, M. C. Moynihan, and A. C. Patel, *Sustainable Materials: with Both Eyes Open*, UIT Cambridge Limited Cambridge, UK, 2012, vol. 2012.
4 I. R. Souza Filho, Y. Ma, D. Raabe and H. Springer, Fundamentals of Green Steel Production: On the Role of Gas Pressure During Hydrogen Reduction of Iron Ores, *JOM*, 2023, **75**(7), 2274–2286.
5 Y. Ma, I. R. Souza Filho, X. Zhang, S. Nandy, P. Barriobero-Vila, G. Requena, D. Vogel, M. Rohwerder, D. Ponge, H. Springer and D. Raabe, Hydrogen-based direct reduction of iron oxide at 700 °C: Heterogeneity at pellet and microstructure scales, *Int. J. Miner., Metall. Mater.*, 2022, **29**(10), 1901–1907.
6 V. Vogl, M. Åhman and L. J. Nilsson, Assessment of hydrogen direct reduction for fossil-free steelmaking, *J. Cleaner Prod.*, 2018, **203**, 736–745.
7 D. Raabe, M. J. Klug, Y. Ma, Ö. Büyükuslu, H. Springer, and I. Souza Filho, in *Hydrogen Plasma Reduction of Iron Oxides, Advances in Pyrometallurgy, Cham*, ed. C. Fleuriault; J. D. Steenkamp; D. Gregurek; J. F. White; Q. G. Reynolds; P. J. Mackey; S. A. C. Hockaday, Springer, Nature Switzerland: Cham, 2023, pp. 83–84.

8 A. Otto, M. Robinius, T. Grube, S. Schiebahn, A. Praktiknjo and D. Stolten, Power-to-Steel: Reducing CO_2 through the Integration of Renewable Energy and Hydrogen into the German Steel Industry, *Energies*, 2017, **10**(4), 451.
9 U. Manzoor, L. Mujica Roncery, D. Raabe and I. R. Souza Filho, Sustainable nickel enabled by hydrogen-based reduction, *Nature*, 2025, **641**, 365–373.
10 F. Gomollón-Bel, Ten Chemical Innovations That Will Change Our World: IUPAC identifies emerging technologies in Chemistry with potential to make our planet more sustainable, *Chem. Int.*, 2019, **41**(2), 12–17.
11 G. Kaupp, Mechanochemistry: the varied applications of mechanical bond-breaking, *CrystEngComm*, 2009, **11**(3), 388–403.
12 V. V. Boldyrev and K. Tkáčová, Mechanochemistry of Solids: Past, Present, and Prospects, *J. Mater. Synth. Process.*, 2000, **8**(3), 121–132.
13 P. Baláž, M. Achimovičová, M. Baláž, P. Billik, Z. Cherkezova-Zheleva, J. M. Criado, F. Delogu, E. Dutková, E. Gaffet, F. J. Gotor, R. Kumar, I. Mitov, T. Rojac, M. Senna, A. Streletskii and K. Wieczorek-Ciurowa, Hallmarks of mechanochemistry: from nanoparticles to technology, *Chem. Soc. Rev.*, 2013, **42**(18), 7571–7637.
14 S. L. James, C. J. Adams, C. Bolm, D. Braga, P. Collier, T. Friščić, F. Grepioni, K. D. M. Harris, G. Hyett, W. Jones, A. Krebs, J. Mack, L. Maini, A. G. Orpen, I. P. Parkin, W. C. Shearouse, J. W. Steed and D. C. Waddell, Mechanochemistry: opportunities for new and cleaner synthesis, *Chem. Soc. Rev.*, 2012, **41**(1), 413–447.
15 P. Baláž, Mechanochemistry in extractive metallurgy: The modern science with old routes, *Acta Metall. Slovaca*, 2001, **4**, 23–28.
16 M. Marchini, G. Montanari, L. Casali, M. Martelli, L. Raggetti, M. Baláž, P. Baláž and L. Maini, "What makes every work perfect is cooking and grinding": the ancient roots of mechanochemistry, *RSC Mechanochem.*, 2024, **1**(1), 123–129.
17 K. J. Kim, K. Sumiyama and K. Suzuki, Ferromagnetic α-Mn type Mn-Al alloys produced by mechanochemical methods, *J. Magn. Magn. Mater.*, 1995, **140–144**, 49–50.
18 L. Diaz Barriga Arceo, J. J. Cruz-Rivera, J. G. Cabañas-Moreno, K. Tsuchiya, M. Umemoto and H. A. Calderón, Characterization of Cu-Co Alloys Produced by Mechanosynthesis and Spark Plasma Sintering, *Mater. Sci. Forum*, 2000, **343–346**, 641–648.
19 V. E. Oliker, V. L. Sirovatka, T. Y. Gridasova, I. I. Timofeeva and A. I. Bykov, Mechanochemical synthesis and structure of Ti-Al-B-based alloys, *Powder Metall. Met. Ceram.*, 2008, **47**(9), 546–556.
20 G. R. Khayati and K. Janghorban, The nanostructure evolution of Ag powder synthesized by high energy ball milling, *Adv. Powder Technol.*, 2012, **23**(3), 393–397.
21 W. Li and K. Sun, A New Technology of Producing Fe-TiC Powder by Mechanical Activation-Reductive Diffusion, *Adv. Mater. Res.*, 2011, **199–200**, 1813–1818.
22 T. Mushove, H. K. Chikwanda, C. Machio and S. Ndlovu, Ti-Mg Alloy Powder Synthesis *via* Mechanochemical Reduction of TiO_2 by Elemental Magnesium, *Mater. Sci. Forum*, 2009, **618–619**, 517–520.
23 G. B. Schaffer and P. G. McCormick, Combustion synthesis by mechanical alloying, *Scr. Metall.*, 1989, **23**(6), 835–838.
24 T. F. Grigoryeva, A. A. Novakova, T. Y. Kiseleva, A. P. Barinova, A. I. Ancharov, T. L. Talako, I. A. Vorsina, K. D. Becker, V. Šepelák, S. V. Tsybulya, O. A. Bulavchenko and N. Z. Lyakhov, Mechanochemical production of nanocomposites of metal/oxide and intermetallic/oxide systems, *J. Phys.: Conf. Ser.*, 2009, **144**(1), 012076.
25 A. Michaely, O. Janka, E. C. J. Gießelmann, R. Haberkorn, H. T. A. Wiedemann, C. W. M. Kay and G. Kickelbick, Black Titania and Niobia within Ten Minutes – Mechanochemical Reduction of Metal Oxides with Alkali Metal Hydrides, *Chem. - Eur. J.*, 2023, **29**(29), e202300223.
26 J. Kano, E. Kobayashi, W. Tongamp and F. Saito, Reduction of Indium(III) Oxide to Indium through Mechanochemical Route, *Chem. Lett.*, 2008, **37**(2), 204–205.
27 F. K. Crundwell, M. S. Moats, V. Ramachandran, T. G. Robinson, and W. G. Davenport, *Extractive Metallurgy of Nickel, Cobalt and Platinum Group Metals*, Elsevier, Oxford, 2011.
28 M. Kowalski and P. J. Spencer, Thermodynamic reevaluation of the C-O, Fe-O and Ni-O systems: Remodelling of the liquid, BCC and FCC phases, *Calphad*, 1995, **19**(3), 229–243.
29 H. Okamoto, Ni-O (nitrogen-oxygen), *J. Phase Equilib.*, 1997, **18**(4), 404.
30 S. Pöyhtäri, J. Ruokoja, E.-P. Heikkinen, A. Heikkilä, T. Kokkonen and P. Tynjälä, Kinetic Analysis of Hydrogen Reduction of Nickel Compounds, *Metall. Mater. Trans. B*, 2024, **55**(1), 251–265.
31 K. V. Manukyan, A. G. Avetisyan, C. E. Shuck, H. A. Chatilyan, S. Rouvimov, S. L. Kharatyan and A. S. Mukasyan, Nickel Oxide Reduction by Hydrogen: Kinetics and Structural Transformations, *J. Phys. Chem. C*, 2015, **119**(28), 16131–16138.
32 T. A. Utigard, M. Wu, G. Plascencia and T. Marin, Reduction kinetics of Goro nickel oxide using hydrogen, *Chem. Eng. Sci.*, 2005, **60**(7), 2061–2068.
33 J. T. Richardson, R. Scates and M. V. Twigg, X-ray diffraction study of nickel oxide reduction by hydrogen, *Appl. Catal., A*, 2003, **246**(1), 137–150.
34 Q. Jeangros, T. W. Hansen, J. B. Wagner, C. D. Damsgaard, R. E. Dunin-Borkowski, C. Hébert, J. Van herle and A. Hessler-Wyser, Reduction of nickel oxide particles by hydrogen studied in an environmental TEM, *J. Mater. Sci.*, 2013, **48**(7), 2893–2907.
35 R. P. Furstenau, G. McDougall and M. A. Langell, Initial stages of hydrogen reduction of NiO(100), *Surf. Sci.*, 1985, **150**(1), 55–79.
36 J. A. Rodriguez, J. C. Hanson, A. I. Frenkel, J. Y. Kim and M. Pérez, Experimental and Theoretical Studies on the Reaction of H_2 with NiO: Role of O Vacancies and Mechanism for Oxide Reduction, *J. Am. Chem. Soc.*, 2002, **124**(2), 346–354.

37 R. Chatterjee, S. Banerjee, S. Banerjee and D. Ghosh, Reduction of Nickel Oxide Powder and Pellet by Hydrogen, *Trans. Indian Inst. Met.*, 2012, **65**(3), 265–273.
38 H. Yang and P. G. McCormick, Mechanically activated reduction of nickel oxide with graphite, *Metall. Mater. Trans. B*, 1998, **29**(2), 449–455.
39 A. M. Padhan, B. Kisan and P. Alagarsamy, Structural, vibrational and magnetic properties of NiO-(Mg,Ti) powders: The effect of reduction reaction, *J. Magn. Magn. Mater.*, 2020, **494**, 165784.
40 A. M. Padhan and P. Alagarsamy, Investigation of NiO reduction dynamics and properties of NiO-Ti powders, *J. Alloys Compd.*, 2020, **840**, 155769.
41 V. Udhayabanu, N. Singh and B. S. Murty, Mechanical activation of aluminothermic reduction of NiO by high energy ball milling, *J. Alloys Compd.*, 2010, **497**(1), 142–146.
42 A. M. Padhan, P. Ravikumar, P. Saravanan and P. Alagarsamy, Enhanced magnetic properties of NiO powders by the mechanical activation of aluminothermic reduction of NiO prepared by a ball milling process, *J. Magn. Magn. Mater.*, 2016, **418**, 253–259.
43 N. Davison, T. Khatun, I. Arce-Garcia, J. A. Gould, J. A. Dawson and E. Lu, Facile Mechanochemical Reduction and Lithium-Ion Doping of Transition-Metal Oxides, *Eur. J. Inorg. Chem.*, 2023, **26**(35), e202300344.
44 S. Doppiu, V. Langlais, J. Sort, S. Suriñach, M. D. Baró, Y. Zhang, G. Hadjipanayis and J. Nogués, Controlled Reduction of NiO Using Reactive Ball Milling under Hydrogen Atmosphere Leading to Ni–NiO Nanocomposites, *Chem. Mater.*, 2004, **16**(26), 5664–5669.
45 J. J. Gilman, Mechanochemistry, *Science*, 1996, **274**(5284), 65.
46 S. Mateti, M. Mathesh, Z. Liu, T. Tao, T. Ramireddy, A. M. Glushenkov, W. Yang and Y. I. Chen, Mechanochemistry: A force in disguise and conditional effects towards chemical reactions, *Chem. Commun.*, 2021, **57**(9), 1080–1092.
47 R. Guan, L. Sheng, C. Li, J. Gu, J.-M. Seo, B.-J. Jang, S.-H. Kim, J. Kim, H. Lim, Q. Li and J.-B. Baek, Mechanochemical carbon dioxide capture and conversion, *Nat. Nanotechnol.*, 2025, **20**, 1247–1253.
48 P. Liu, H. Chen, H. Yu, X. Liu, R. Jiang, X. Li and S. Zhou, Oxygen vacancy in magnesium/cerium composite from ball milling for hydrogen storage improvement, *Int. J. Hydrogen Energy*, 2019, **44**(26), 13606–13612.
49 X. Liu, H. Wen, B. Guo, C. Lv, W. Shi, W. Kang, J. Zhang, R. Yuan and C. Zhang, Pan-Milling: Instituting an All-Solid-State Technique for Mechanical Metastable Oxides as High-Performance Lithium-Ion Battery Anodes, *Adv. Energy Mater.*, 2021, **11**(14), 2100310.
50 W. Wu, H. Fang, H. Ma, L. Wu, Q. Wang and H. Wang, Self-Powered Rewritable Electrochromic Display based on WO_{3-x} Film with Mechanochemically Synthesized MoO_{3-y} Nanosheets, *ACS Appl. Mater. Interfaces*, 2021, **13**(17), 20326–20335.
51 J. M. McKay and V. E. Henrich, Surface electronic structure of NiO: Defect states, O_2 and H_2O interactions, *Phys. Rev. B:Condens. Matter Mater. Phys.*, 1985, **32**(10), 6764–6772.
52 T. Hidayat, M. A. Rhamdhani, E. Jak and P. C. Hayes, Investigation of Nickel Product Structures Developed during the Gaseous Reduction of Solid Nickel Oxide, *Metall. Mater. Trans. B*, 2009, **40**(4), 462–473.
53 S. Reichle, M. Felderhoff and F. Schüth, Mechanocatalytic Room-Temperature Synthesis of Ammonia from Its Elements Down to Atmospheric Pressure, *Angew. Chem., Int. Ed.*, 2021, **60**(50), 26385–26389.
54 C. L. Cronan, F. J. Micale, A. C. Zettlemoyer, M. Topic and H. Leidheiser, Surface properties of $Ni(OH)_2$ and NiO. III. Microporosity and irreversible water adsorption of NiO prepared by thermal decomposition of $Ni(OH)_2$, *J. Colloid Interface Sci.*, 1980, **75**(1), 43–50.
55 X. Zhang, A. He, R. Guo, Y. Zhao, L. Yang, S. Morita, Y. Xu, I. Noda and Y. Ozaki, A new approach to removing interference of moisture from FTIR spectrum, *Spectrochim. Acta, Part A*, 2022, **265**, 120373.
56 Y. Sawama, M. Niikawa, Y. Yabe, R. Goto, T. Kawajiri, T. Marumoto, T. Takahashi, M. Itoh, Y. Kimura, Y. Sasai, Y. Yamauchi, S.-i. Kondo, M. Kuzuya, Y. Monguchi and H. Sajiki, Stainless-Steel-Mediated Quantitative Hydrogen Generation from Water under Ball Milling Conditions, *ACS Sustainable Chem. Eng.*, 2015, **3**(4), 683–689.
57 S. Mori, W. C. Xu, T. Ishidzuki, N. Ogasawara, J. Imai and K. Kobayashi, Mechanochemical activation of catalysts for CO_2 methanation, *Appl. Catal., A*, 1996, **137**(2), 255–268.
58 O. S. Morozova, A. N. Streletskii, I. V. Berestetskaya and A. B. Borunova, Co and Co_2 hydrogenation under mechanochemical treatment, *Catal. Today*, 1997, **38**(1), 107–113.
59 A. Barakat, M. Al-Noaimi, M. Suleiman, A. S. Aldwayyan, B. Hammouti, T. B. Hadda, S. F. Haddad, A. Boshaala and I. Warad, One Step Synthesis of NiO Nanoparticles *via* Solid-State Thermal Decomposition at Low-Temperature of Novel Aqua(2,9-dimethyl-1,10-phenanthroline)$NiCl_2$ Complex, *Int. J. Mol. Sci.*, 2013, **14**(12), 23941–23954.
60 D. S. Lee and D. J. Min, A Kinetics of Hydrogen Reduction of Nickel Oxide at Moderate Temperature, *Met. Mater. Int.*, 2019, **25**(4), 982–990.
61 P. Baláž, *Mechanochemistry in Nanoscience and Minerals Engineering*, Springer, Berlin, Heidelberg, 2008, XIII, p. 413.
62 P. Baláž, *Extractive Metallurgy of Activated Minerals*, Elsevier, 2000, vol. 10.
63 X. Zhao, Y. Ding, L. Ma, X. Shen and S. Xu, Structure, morphology and electrocatalytic characteristics of nickel powders treated by mechanical milling, *Int. J. Hydrogen Energy*, 2008, **33**(21), 6351–6356.